Combined Experimental Studies and Theoretical Calculations To Yield the Complete Molecular Structure and Vibrational Spectra of $(CH_3)_3GeH$

María L. Roldán,[†] Silvia A. Brandán,[†] Sarah L. Masters (née Hinchley),[‡] Derek A. Wann,[‡] Heather E. Robertson,[‡] David W. H. Rankin,[‡] and Aída Ben Altabef*,[†]

INQUINOA, CONICET, Instituto de Química Física, Facultad de Bioquímica, Química y Farmacia, Universidad Nacional de Tucumán, San Lorenzo 456, T4000CAN Tucumán, R. Argentina, and School of Chemistry, University of Edinburgh, West Mains Road, Edinburgh, EH9 3JJ U.K.

Received: December 11, 2008; Revised Manuscript Received: February 13, 2009

The molecular structure of trimethylgermane has been determined by gas electron diffraction experiments. Infrared spectra for the gaseous, liquid, and solid phases were also recorded. Parallel and perpendicular polarized Raman spectra for the liquid were measured to obtain depolarization values. The experimental studies were supported by a series of computational calculations using HF, B3LYP, and MP2 methods and a variety of basis sets. The force fields obtained from density functional theory using both B3LYP/6-31G* and B3LYP/6-311+G** were scaled with both Pulay's SQM methodology and Yoshida's WLS procedure to simulate the vibrational spectra and assist in the assignment of fundamental bands. The Raman intensities were obtained from polarizability derivatives. The vibrational spectra of trimethylgermane were completely assigned on the basis of the experimental data and the theoretical prediction of vibrational frequencies and intensities.

Introduction

Both halogen-substituted trimethylgermanes and trimethylgermane (TMG) itself are frequently used in organic synthesis.[1−5] Interesting applications are known for TMG, for example, in coupling reactions catalyzed by ruthenium to obtain polygermanes. These display electrical and optical properties usually not observed in saturated polymers, such as the λ_{max} shift to red with chain length increment, narrow emission bands and semiconducting behavior.[6] In addition, TMG can be used as a precursor, providing a source of germanium that is then reacted and used for the deposition of GeSbTe thin films by chemical vapor deposition (CVD) processes, which are applied to electronic devices.[7] The reaction of TMG with hydrogen is believed to play an important role in the CVD process used in the semiconductor industry.[8] Kinetic studies on the series $(CH_3)_{(4-n)}GeH_n$ ($n = 1-4$) reveals that the reactivity of these species increases when methyl substitution increases from GeH_4 to $(CH_3)_3GeH$ due to a reduction in the strength of the Ge−H bond.[8,9] Because the reactivity of TMG is intimately related to its structure, a reliable study of its molecular geometry and vibrational properties is essential. A partial structural study of TMG was carried out by Durig et al.[10] using microwave spectroscopy. To obtain a complete molecular structure, we have studied the molecule using gas-phase electron diffraction (GED) in combination with quantum chemical calculations.

The vibrational spectra of TMG were previously investigated by Van de Vondel et al.[11] Later, Imai et al.[12] carried out a normal coordinate analysis for TMG and its deuterated derivatives. A number of studies involving the GeH stretching frequencies have also appeared in the literature.[13−15] As some vibrational modes were not observed or were assigned to a single frequency in previous studies,[11,12] a more detailed study of the vibrational spectra for TMG is presented in this work. IR spectra for the gas, liquid, and solid phases and Raman spectra for the liquid were measured for TMG. The experimental data are augmented by an analysis based on the harmonic force field calculation, providing frequency and intensity values that can be used to simulate the experimental spectra. To obtain an accurate prediction, the harmonic frequencies obtained from the theoretical calculations were scaled using both the scaled quantum mechanical (SQM) method developed by Pulay et al.[16−19] and the wavenumber linear scaling (WLS) method derived by Yoshida et al.[20] Raman intensities were estimated on the basis of polarizabilities derived with respect to the Cartesian coordinates, whereas infrared intensities were obtained from the calculations. The depolarization ratios and the additional data obtained from the Fourier self-deconvolution (FSD) and curve-fitting analysis along with the data predicted from calculations provide a complete assignment for the experimental spectra.

Experimental Methods

Trimethylgermane was purchased from ABCR and handled under inert conditions to avoid exposure to atmospheric humidity.

Gas Electron Diffraction. Data were collected for TMG using the Edinburgh gas-phase electron diffraction apparatus.[21] An accelerating voltage of around 40 kV was used, representing an electron wavelength of approximately 6.0 pm. Scattering intensities were recorded on Kodak Electron Image films at nozzle-to-film distances of 285.23 and 127.75 mm, with sample and nozzle temperatures held at 293 K. The weighting points for the off-diagonal weight matrices, correlation parameters and scale factors for both camera distances for trimethylgermane are given in Table S1, Supporting Information. Also included are the electron wavelengths, as determined from the scattering patterns for benzene, which were recorded immediately after the patterns for the sample compounds. The scattering intensities were measured using an Epson Expression 1680 Pro flatbed scanner and converted to mean optical densities as a function

* Corresponding author. Tel.: +54 381 4311044. Fax: +54 381 4248169. E-mail: altabef@fbqf.unt.edu.ar. Member of the Carrera del Investigador Científico, CONICET (R. Argentina).
[†] Universidad Nacional de Tucumán.
[‡] University of Edinburgh.

10.1021/jp810988s CCC: $40.75
Published on Web 03/19/2009

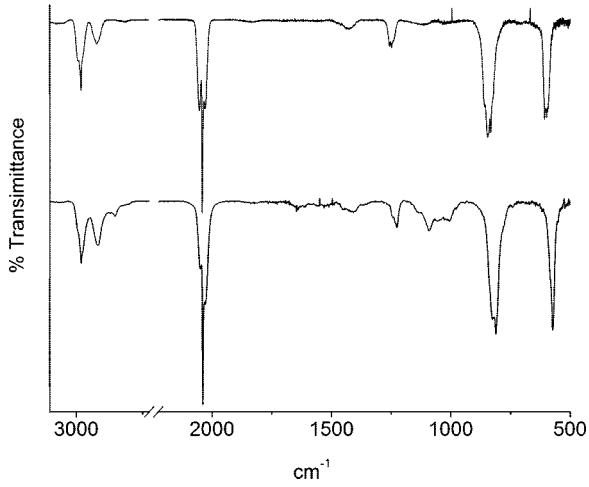

Figure 1. Experimental infrared spectra for the gas and the liquid phase.

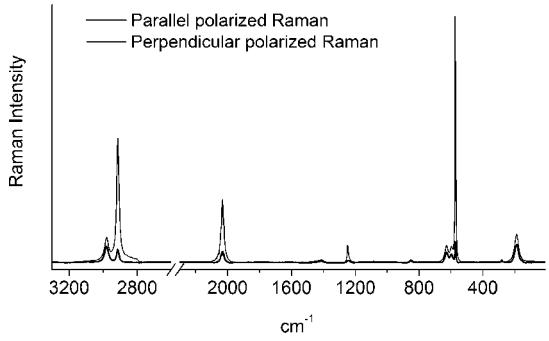

Figure 2. Overlaid parallel and perpendicular polarized Raman spectra.

of the scattering variable, s, using an established program.[22] The data reduction and the least-squares refinement processes were carried out using the ed@ed program[23] employing the scattering factors of Ross et al.[24]

Raman and Infrared Spectroscopy. The infrared spectra for gaseous, liquid, and solid TMG were recorded on a FTIR spectrophotometer (Perkin-Elmer Model GX1) in the range 4000−400 cm^{-1}. The FTIR spectrum of the gas sample was obtained by using a 10 cm path length cell with Si windows, with a resolution of 1 cm^{-1} and 64 scans; the liquid spectrum was registered as a film between KBr windows, with a resolution of 2 cm^{-1} and 64 scans. A variable temperature RIIC (VLT-2) cell equipped with AgCl windows was used to obtain the low-temperature infrared spectra. The measurements were made at different temperatures by cooling the liquid sample from room temperature (298 K) to liquid nitrogen temperature (100 K). The gas and liquid infrared spectra are shown in Figure 1 whereas the low temperature spectra are displayed further on. The parallel and perpendicular polarized Raman spectra for the liquid sample (Figure 2) were recorded with an FT-Raman Bruker RFS 100 spectrophotometer, equipped with a Nd:YAG laser with excitation line of 1064 nm and a liquid N_2-cooled Ge detector, using a resolution of 1 cm^{-1} and 200 scans. The depolarization values were obtained from the intensity ratios of the fundamental bands in both spectra, without calibration with CCl_4. The observed bands in the IR and Raman spectra and the assignment to the vibrational normal modes of the molecule are listed in Table 1.

Spectral Analysis. Fourier self-deconvolution (FSD)[25] and curve fitting[26] were applied to the Raman spectra to enhance the resolution of the spectral profile. Following the approach used by previous authors,[27,28] the estimated band positions were obtained from the application of FSD to the baseline-corrected spectrum. Curve fitting of the FSD spectra gives accurate frequencies and positions of the component bands. The criterion for acceptance of the resulting bands was the consistency between curve fitting of the baseline-corrected experimental spectrum, using the frequency positions and initial band shapes, and the deconvoluted fitted spectrum. Analysis of the vibrational spectra was performed using the standard software of the infrared spectrophotometer[29] and Gaussian band shapes.

Computational Methods. The structure of the molecule was investigated using C_{3v} symmetry. An experimental gas-phase investigation of iodotrimethylsilane revealed that allowing the structure freedom to deviate from C_{3v} to C_3 symmetry caused no change to the structure,[30] whereas the related iodotrimethylgermane was also modeled with C_{3v} symmetry.[31] Therefore, trimethylgermane was modeled with C_{3v} symmetry only. Calculations were performed using the Gaussian03 program.[32]

A series of calculations combining the HF, hybrid functional B3LYP or MP2 methods with the 6-31G, 6-31G*, 6-31+G, 6-31+G*, 6-311G, 6-311G*, 6-311+G, 6-311+G*, 6-311G**, 6-311+G**, 6-311++G**, Lanl2dz (ECP), Lanl2dzdp (ECP), cc-pVTZ and cc-pVTZ basis sets was used to calculate the vibrational frequencies, infrared intensities and Raman scatterings. These calculations determined the best theoretical approximation to predict the vibrational frequencies. The parameters obtained with the split-valence basis sets are given in Table S2, Supporting Information.

Estimates of the amplitudes of vibration (u_{h1})[33] for use in the GED refinement were also required. The analytic second derivatives of the energy with respect to the nuclear coordinates calculated at the MP2 level with the 6-311++G** basis set gave force fields, which were used to provide these estimates.

Although the GED vibrational analysis was carried out with MP2 method, the vibrational spectra assignment was based on B3LYP. The latter has demonstrated overall accuracy for a variety of systems and all the scaling methods were defined for this level of calculation.

The harmonic force field in Cartesian coordinates obtained from the B3LYP/6-31G* calculation was converted to local C_{3v} symmetry coordinates for the methyl groups and also for the GeC_3 group. These coordinates were expressed as linear combinations of internal coordinates following the method described by Fogarasi and Pulay[34] and were defined as shown in Table S3, Supporting Information. The resulting force field was scaled using Pulay's SQM methodology,[16−19] in which the diagonal force constants associated with each symmetry coordinate are multiplied by a small number of scale factors ($f_i, f_j,...$). These scale factors are optimized, minimizing the mean square deviations between the calculated and observed frequencies, until reaching the best agreement between the calculated and the experimental frequencies. Consequently, the off-diagonal constants are automatically scaled by the geometrical mean of factors $[(f_i \cdot f_j)^{1/2}]$ corresponding to the diagonal constants. For the inactive A_2 modes, zero weighing factors were assigned. The scaled quantum mechanical (SQM) force field was used to obtain the scaled frequencies, the potential-energy distribution (PED) and the internal valence force constants. The force constants conversion, fitting of the scale factors and PED calculation was carried out with the FCARTP program.[35]

To obtain a satisfactory description of the observed spectra, Raman intensities were calculated, converting the Raman activities (S_i) obtained from the Gaussian03 program[32] to relative Raman intensities, I_i, using the following relationship:[36] $I_i =$

TABLE 1: Observed Bands in Infrared and Raman Spectra of Trimethylgermane

infrared[a]						Raman[c]				
		liquid								
gas		room temperature		low temperature[b]		observed[d]		depolarization ratios[e]		assignment[f]
2994	sh	2991		2980	sh					ν_{13}
2986	sh	2982	m	2975	s	2980	(34)	dp	0.72	ν_1
2983	s	2978	sh	2972	sh					ν_{14}
2924	s	2919	m	2911	s	2913	(100)	p	0.13	ν_2
2916	sh	2916	sh							ν_{15}
2040	vs	2041	vs	2042	s	2032	(39)	p	0.27	ν_3
1436	sh			1426		1441[f]	sh			ν_4
1425	w	1420	w	1415	m	1414[f]	(2)	dp	0.75	ν_{16}
1414	sh			1393		1384[f]	sh			ν_{17}
1256	sh	1256	sh	1238	vs	1248	(7)	p	0.13	ν_5
1247	m	1244	m	1234		1235	sh			ν_{18}
845	s	846	s	850	vs	853[f]	(2)	dp	0.75	ν_{19}
833		832		831		840[f]	sh			ν_6
827	sh			825		828[f]	sh			ν_{20}
				626	w	629	(12)	dp	0.68	ν_{21}
598	s	598	s	598	vs	600	(11)	dp	0.63	ν_{22}
575	w	575	w	574	s	575	(77)	p	0.11	ν_7
						190	(17)	dp	0.72	ν_{23}
						132	(2)			ν_{24}

[a] Key: w, weak; m, medium; s, strong; vs, very strong; vw, very weak; sh, shoulder. [b] From the infrared spectrum of a sample cooled in liquid nitrogen. [c] Relative intensity in parentheses. [d] Depolarized ratio: p, polarized; dp, depolarized. [e] Key: ν, stretching; δ, angular deformation; ρ, rocking; τ, torsion; s, symmetric; a, antisymmetric. [f] From Fourier self-deconvolution and curve-fitting.

$f(\nu_o - \nu_i)^4 hcS_i/\nu_i[1 - \exp(-hc\nu_i/kT)]$, where ν_o is the excitation frequency (in cm^{-1}), ν_i is the vibrational frequency (in cm^{-1}) of the ith normal mode, h, k, and c are Planck's constant, the Boltzmann constant, and the universal velocity constant, respectively, and f is a suitably chosen normalization factor for all the peak intensities. The infrared intensities were taken directly from the calculations. The experimental spectral profile for both the infrared and Raman spectra was simulated using Lorentzian band shapes and a mean γ value of 12 cm^{-1}.[37]

Results and Discussion

Computational Investigation. The molecular structure of Me_3GeH was investigated with a range of ab initio and DFT methods and a wide assortment of basis sets. All calculations agree that the molecule has C_{3v} symmetry, with most bond lengths and angles not varying significantly. Only bond length parameters involving germanium showed a large difference among basis sets for all methods. For example, the Ge−C bond length was predicted to increase by ~1.7 pm between the 6-31G*/6-31+G* double-ζ and the 6-311G* triple-ζ basis sets, whereas the Ge−H bond length was predicted to shorten by ~1.3 pm. All other parameters showed little variation between basis sets for each method and only small differences between methods (see Table S2, Supporting Information).

The computed molecular dipole from the HF, B3LYP, and MP2 methods, all with the 6-311++G** basis set, were 0.48, 0.48, and 0.45 D, respectively. These compare reasonably well with the experimental value of 0.67 D.[38] These values indicate that the molecule is not very polar, with only a small permanent dipole.

Gas electron diffraction. On the basis of the ab initio calculations described above, electron-diffraction refinements were carried out using a model with overall C_{3v} symmetry to describe the gaseous structure, shown in Figure 3 with the atom numbering. The structure was defined in terms of six independent parameters, comprising three bond lengths, two bond angles and a tilt of the methyl groups. The bond lengths were rC−H (p_1), rGe−C (p_2), and rGe−H (p_3). A single C−H bond length

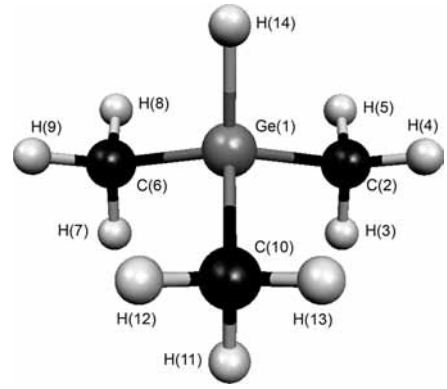

Figure 3. Molecular geometry of Me_3GeH showing atom labeling.

was used because the individual ab initio values differed by no more than 0.1 pm. The model also required two angle parameters, ∠Ge−C−H (p_4) and ∠H−Ge−C (p_5), providing local C_{3v} symmetry for the methyl groups. The methyl tilt parameter was also included and a positive tilt indicated a decrease of the unique ∠Ge−C−H and an increase of the pair of symmetry-related ∠Ge−C−H, i.e., away from the Ge−H bond. The starting parameters for the r_{h1} refinement[33] were taken from the theoretical geometry optimized at the MP2/6-311++G** level. A theoretical (MP2/6-311++G**) Cartesian force field was obtained and converted into a force field described by a set of symmetry coordinates using the program SHRINK.[33] From this, the rms amplitudes of vibration (u_{h1})[33] and the perpendicular distance corrections (k_{h1})[33] were generated at the harmonic first-order curvilinear motion approximation. All geometric parameters and five groups of amplitudes of vibration were then refined using the SARACEN method,[39] with flexible restraints employed for two parameters and one amplitude of vibration. The rotation constant from microwave spectroscopy was also included as an extra observation.[10]

The final refinement for trimethylgermane provided a satisfactory fit to the data, with $R_G = 0.064$ ($R_D = 0.033$), and can be assessed on the basis of the radial-distribution curve (Figure

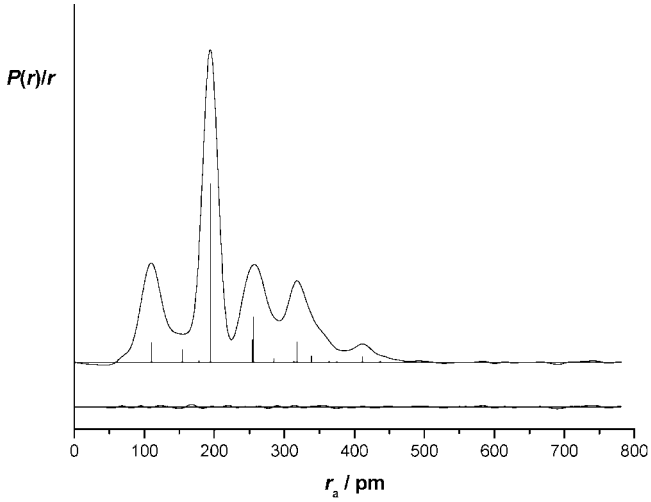

Figure 4. Experimental and difference (experimental − theoretical) radial-distribution curves, $P(r)/r$, for Me_3GeH. Before Fourier inversion the data were multiplied by $s \cdot \exp(-0.00002s^2)/(Z_{Ge} - f_{Ge})(Z_C - f_C)$.

4) and the molecular-scattering intensity curves (Figure S1, Supporting Information). Final refined parameters are listed in Table 2. The interatomic distances and corresponding rms amplitudes of vibration are given in Table S4 (Supporting Information). The least-squares correlation matrix is given in Table S5 (Supporting Information) and the coordinates of the final refined structure from the GED investigation are given in Table S6 (Supporting Information).

The molecular structure of $(CH_3)_3Ge-H$ can be compared to those determined by GED for $(CH_3)_3Ge-X$ [(X = Cl, Br, or I); Table S7 (Supporting Information)].[31,40] In these cases, C_{3v} symmetry was returned for all molecules, and ab initio calculations agreed that this high level of symmetry was a minimum on the potential-energy surface. Ge−C bond lengths (r_g) of 195.0(4) pm (X = Cl), 195.2(7) pm (X = Br), and 194.3(1) pm (X = I) were observed experimentally, whereas 194.7(1) pm was observed in this work. Therefore, no real trend can be established for the Ge−C bond lengths; they are all in the region of 194−195 pm and the substituent, regardless of whether it is a halogen or not, does not appear to have much effect on the parameter.

The computational investigation at all levels (HF, DFT, MP2) with triple-ζ basis sets overestimated the Ge−C bond lengths compared to the experimental result. For example, B3LYP/6-311++G** indicated a Ge−C bond length of 197.4 pm compared to the r_{h1} value of 194.77(4) pm. Distances of 196.7 and 196.4 pm were obtained from HF and MP2 with the same basis set. Double-ζ basis sets performed much better, for example, the MP2/6-31+G* calculation predicted 194.7 pm, agreeing with experiment.

The experimental X−Ge-C angles can be compared, with ∠H−Ge−C = 108.7(1)°, ∠Cl−Ge−C = 106.0(8)°, ∠Br−Ge−C = 104.2(13)° and ∠I−Ge−C = 105.5(2)° all being observed by gas diffraction methods. A definite decrease of 3° between the nonhalogenated and halogenated species can be observed, but within the halogenated species, no discernible trend is observed.

The gaseous molecular structure of dimethylgermane is also known.[41] In this case, rGe−C is 195.0(3) pm and ∠C−Ge−C is 110.0(5)° from gas electron diffraction, whereas in trimethylgermane, rGe−C = 194.67(4) pm and ∠C−Ge−C = 110.2(1)°. Thus the increase in methyl substituents leads to little change within the overall molecular structure, implying that neither structure is sterically strained. For digermane (Ge_2H_6),[42] Ge−H bond lengths of 154.1(6) pm are observed, compared to 154.4(4) pm for trimethylgermane, whereas in hexamethyldigermane,[43] Ge−C bond lengths of 195.7(1) pm are observed, compared to 194.67(4) pm from our study.

The structure of TMG has been studied previously using rotational spectroscopy.[10] We are able to extract rotational constants from our diffraction refinement programs and compare them to those obtained from a microwave study. In this case, the microwave study determined a rotation constant of 4785.88 MHz, compared to a value of 4782.91(1.71) MHz for the GED structure. These values compare well, as do the structural parameters from both studies.

Spectroscopic Analysis. For TMG (C_{3v} symmetry, Figure 3), the normal coordinate analysis predicts 36 vibrational normal modes classified as $8A_1$ (IR, Ra) + $4A_2$ + 12E (IR, Ra). The A_1 and E modes are infrared and Raman active, whereas the A_2 modes are forbidden in both spectra by selection rules. The calculated harmonic frequencies obtained from the systematic evaluation of the theoretical calculations are listed in Table S8 (Supporting Information), where they are compared with the experimental data. Because both HF and MP2 methods show larger deviations in comparison with the B3LYP hybrid method, only the results obtained for this level of calculation are presented in Table S8 (Supporting Information). The deviation of the calculated frequencies from experimental frequencies is expressed as the root-mean-square deviation (rmsd). The bands observed for the gas-phase and Raman spectra were used as a reference. From the comparison of all basis sets explored, the 6-311G basis set supplemented with diffuse and polarization functions offers the best description of the vibrational frequencies. For example, the 6-311G**, 6-311+G**, and 6-311++G** basis sets presented the lowest rmsd values with no scaling (67, 66, and 66 cm^{-1}, respectively). Dunning's cc-pVDZ and cc-pVTZ basis sets predict sets of frequencies with the same accuracy as those given by the augmented 6-311G basis sets (rmsd = 67 cm^{-1} and rmsd = 66 cm^{-1}, respectively), whereas the use of ECP basis sets only introduced a slight improvement with the inclusion of polarization functions through the LanL2dzdp basis set (rmsd = 63 cm^{-1}), which shows a better prediction for stretching vibrations involving germanium atoms.

Theoretical Prediction of the Vibrational Spectrum. Theoretical frequencies and band intensities obtained directly from the calculations can be used to simulate the IR and Raman spectra which, when compared to the experimental spectra, provide useful information for the vibrational analysis. However, the values of these frequencies can display large deviations with respect to experimental ones, mainly due to vibrational anharmonicity and calculation deficiencies. Therefore, with the goal of bringing the theoretical calculation of force fields into better agreement with experimental frequencies, scaling procedures were applied to the calculated frequencies. In a first step, the multiple scaled quantum mechanical (SQM)[16−19] methodology (described in the Computational Investigation section) was used to predict the vibrational spectra. Two sets of scale factors available in the literature, proposed by Rauhut and Pulay[17] and Kalincsák and Pongor,[19] were used to scale the 6-31G* force field. The frequencies predicted by these two sets of scale factors are shown in Table 3 along with the experimental and calculated values, and the assignment proposed from the calculation. Second, the wavenumber-linear scaling (WLS) method, proposed by Yoshida et al.,[20] was used to scale the B3LYP/6-311+G** harmonic force field for TMG. This methodology is based on calculating the scale factors as the ratio ν_{obs}/ν_{calc} by

TABLE 2: Refined and Calculated Geometric Parameters for Me_3GeH (Distances in pm, Angles in deg) from the SARACEN GED Study[a,b]

	parameter	GED (r_{h1})	MP2/6-311++G** (r_e)	restraint
		Independent Parameters		
p_1	rC−H	110.8(2)	109.4	
p_2	rGe(1)-C(2/6/10)	194.67(4)	196.4	
p_3	rGe(1)−H(14)	154.4(4)	154.4	154.4(5)
p_4	∠Ge−C−H	110.8(2)	110.6	
p_5	∠H(14)−Ge(1)−C(2/6/10)	108.7(1)	109.2	
p_6	Me tilt	0.5(8)		0.5(10)
		Dependent Parameter		
dp_1	∠C−Ge−C	110.2(1)	109.7	

[a] Figures in parentheses are the estimated standard deviations of the last digits. [b] See Supporting Information for parameter definitions.

TABLE 3: Experimental, Calculated, and Predicted Frequencies after Scaling with Different Sets of Scale Factors

			B3LYP/6-31G*						B3LYP/6-311+G**					
mode	exp	Imai et al.[a]	calc	Rauhut and Pulay[b]	Kalincsák and Pongor[c]	SQM[d]	IR int[e]	Raman int[e]	calc	Yoshida[f]	IR int[e]	Raman int[e]	PED (>10%)	assignment[g]
A_1														
ν_1	2986	2982	3136	3008	3008	2992	36.0	239.4	3109	2978	36.5	259.6	33% S_1 + 66% S_{14}	ν_a CH_3
ν_2	2924	2992	3057	2932	2932	2916	6.0	481.6	3032	2909	6.0	758.9	33% S_2 + 65% S_{15}	ν_s CH_3
ν_3	2040	2040	1981	1900	1918	2040	173.0	338.5	2088	2035	183.0	491.3	100% S_3	ν GeH
ν_4	1436	1426	1521	1455	1454	1430	5.4	0.4	1478	1455	11.0	0.4	31% S_4 + 51% S_{17}	δ_a CH_3
ν_5	1256	1246	1325	1267	1268	1254	1.5	9.0	1285	1270	2.4	75.3	34% S_5 + 69% S_{18}	δ_s CH_3
ν_6	833	833	876	841	849	834	98.0	35.2	852	848	51	0.7	25% S_6 + 29% S_{19} + 38% S_{22}	ρ CH_3 + ν_a GeC_3
ν_7	575	571	584	561	596	581	2.5	289.5	555	555	2.6	412.7	99% S_7	ν_s GeC_3
ν_8	−	187	172	171	188	187	1.1	17.1	183	184	2.4	35.1	118% S_8	δ_s GeC_3
A_2														
ν_9			3140	3012	3013	2996	0.0	0.0	3111	2980	0.0	0.0	34% S_9 + 67% S_{13}	ν_a CH_3
ν_{10}			1508	1443	1443	1419	0.0	0.0	1460	1438	0.0	0.0	32% S_{10} + 51% S_{16}	δ_a CH_3
ν_{11}			749	716	717	704	0.0	0.0	717	715	0.0	0.0	38% S_{11} + 48% S_{20}	ρ CH_3
ν_{12}			116	106	106	104	0.0	0.0	119	120	0.0	0.0	47% S_{12} + 58% S_{24}	τ CH_3
E														
ν_{13}	2994	2982	3141	3013	3014	2997	20.8	179.4	3112	2981	20.8	203.4	34% S_9 + 67% S_{13}	ν_a CH_3
ν_{14}	2983	2982	3134	3006	3006	2990	3.0	28.3	3107	2977	2.0	39.3	33% S_1 + 66% S_{14}	ν_a CH_3
ν_{15}	2916	2922	3055	2931	2931	2916	13.0	0.1	3031	2908	18.5	0.3	33% S_2 + 65% S_{15}	ν_s CH_3
ν_{16}	1425	1426	1518	1453	1452	1428	1.5	15.3	1471	1449	5.0	11.5	32% S_{10} + 51% S_{16}	δ_a CH_3
ν_{17}	1414	1426	1506	1440	1440	1417	<0.1	131.5	1464	1442	<0.1	39.5	31% S_4 + 51% S_{17}	δ_a CH_3
ν_{18}	1247	1246	1318	1261	1264	1248	6.5	0.5	1274	1259	12.1	17.2	34% S_5 + 69% S_{18}	δ_s CH_3
ν_{19}	845	624	886	849	862	844	9.5	55.5	861	857	31.6	39.1	25% S_6 + 29% S_{19} + 38% S_{22}	ρ CH_3 + ν_a GeC_3
ν_{20}	827	833	873	837	854	835	64.0	21.0	848	843	72.0	0.7	38% S_{11} + 48% S_{20}	ρ CH_3
ν_{21}	629	850	629	620	685	629	<0.1	62.3	615	614	6.2	84.1	91% S_{21}	δ_a GeC_3
ν_{22}	598	592	612	592	613	599	40.4	30.5	586	585	44.0	88.6	36% S_{19} + 72% S_{22}	ρ CH_3 + ν_a GeC_3
ν_{23}	190	187	183	182	200	190	0.8	64.4	170	172	1.4	127.7	128% S_{23}	ρ GeC_3
ν_{24}	132		149	136	136	134	<0.1	1.4	127	128	<0.1	2.0	47% S_{12} + 58% S_{24}	τ CH_3
rmsd $(cm^{-1})^h$			85	36	36	4			66	15				

[a] From ref 12. [b] Scaled by using Rauhut and Pulay's scale factors, taken from ref 17. [c] Scaled by using Kalincsák and Pongor's scale factors, taken from ref 19. [d] Calculated using the refinement scale factors of this work. [e] Calculated IR intensities in km mol^{-1} and calculated Raman intensities in $Å^4$ $(amu)^{-1}$. [f] Scaled with Yoshida's equation, from ref 20. [g] Key: ν, stretching; δ, angular deformation; ρ, rocking; τ, torsion; s, symmetric; a, antisymmetric. [h] The inactive A_2 modes were not included in the calculation of the root-mean square deviation (rmsd).

using the following linear equation: $\nu_{obs}/\nu_{calc} = 1.0087(9) - 0.0000163(6)\nu_{calc}$, where ν_{obs} and ν_{calc} are given in cm^{-1}. The WLS method, unlike SQM scaling, was derived for a wide range of molecules including Ge-containing compounds. The scaled frequencies along with the unscaled values for the 6-311+G** force field are also included in Table 3.

The relative infrared and Raman intensities were obtained using the aforementioned procedure to complement the theoretically predicted frequencies, providing a complete computational simulation of the vibrational spectra. These results are collected in Table 3 for both B3LYP/6-31G* and B3LYP/6-311+G**. The scaled infrared and Raman spectra obtained from both SQM and WLS scaling methods, along with the calculated intensities, are shown in Figures 5 and 6, respectively, where they are compared to the experimental ones. Generally, the simulated spectra resemble the observed experimental spectra, providing useful support for the assignment of the vibrational bands to the fundamental modes. Because anharmonicity is larger for the bond stretching involving hydrogen atoms, the unscaled frequencies for B3LYP/6-31G* and 6-311+G** show larger deviations in this region compared to the experimental frequencies, as can be seen in Table 3. The prediction of the C−H and Ge−H stretching vibrations is much better for Yoshida's scaling than for the other methods. For the infrared and Raman intensities, the B3LYP/6-311+G** spectral profile agrees better with the experimental vibrational spectra than the same method with the 6-31G* basis set.[44] Both dipole moments and polarizability derivatives are sensitive to the functional and basis sets used, and basis sets augmented by additional functions such as polarization and diffuse functions are needed for a successful description.

Band Assignments. The assignment of experimental frequencies to the normal modes of vibration was based on comparison with the previous assignment for this molecule,[12]

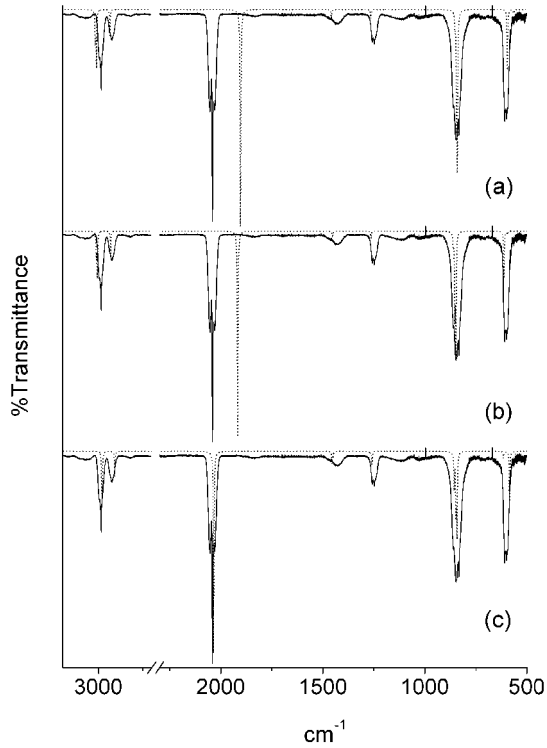

Figure 5. Experimental (thick line) and predicted (thin line) IR spectra of TMG by the SQM method from B3LYP/6-31G* force field using (a) Rauhut and Pulay's scale factors, (b) Kalincsák and Pongor's scale factors, and (c) the wavenumber linear scaling of Yoshida from B3LYP/6-311+G**.

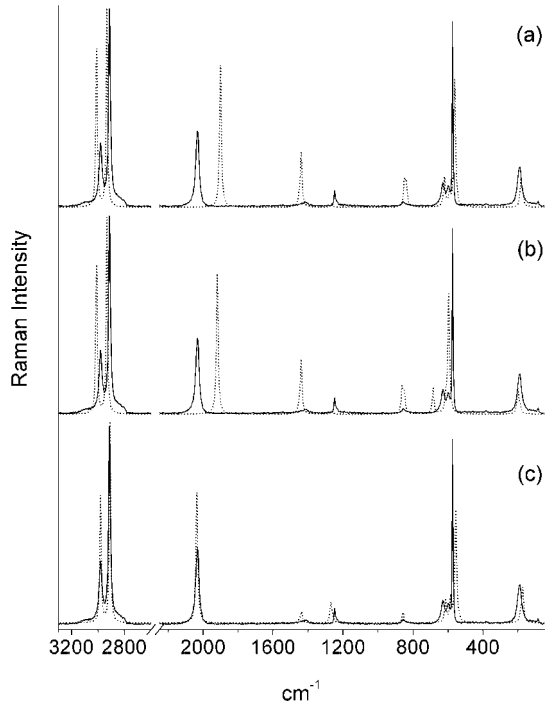

Figure 6. Experimental (thick line) and predicted (thin line) Raman spectra of TMG by the SQM method from B3LYP/6-31G* force field using (a) Rauhut and Pulay's scale factors, (b) Kalincsák and Pongor's scale factors, and (c) the wavenumber linear scaling of Yoshida from B3LYP/6-311+G**.

the assignments reported for related molecules,[31] depolarization ratios and normal mode descriptions, as well as the relative positions and intensities of the bands predicted from the calculations. Because Yoshida's scaling with B3LYP/6-311+G** performed well for the calculation of vibrational frequencies and relative intensities when compared with experimental data, these results were used as a reference for the assignment of the observed bands to the fundamental modes. The experimental bands observed in the IR and Raman spectra, along with their relative intensities and depolarization ratios, are collected in Table 1. The infrared spectra for the gas, liquid, solid phases and the WLS-scaled infrared spectrum using calculated intensities are shown in Figures 7−10 for the regions 3050−2850, 1500−1150, 960−500, and 2120−960 cm^{-1}, respectively.

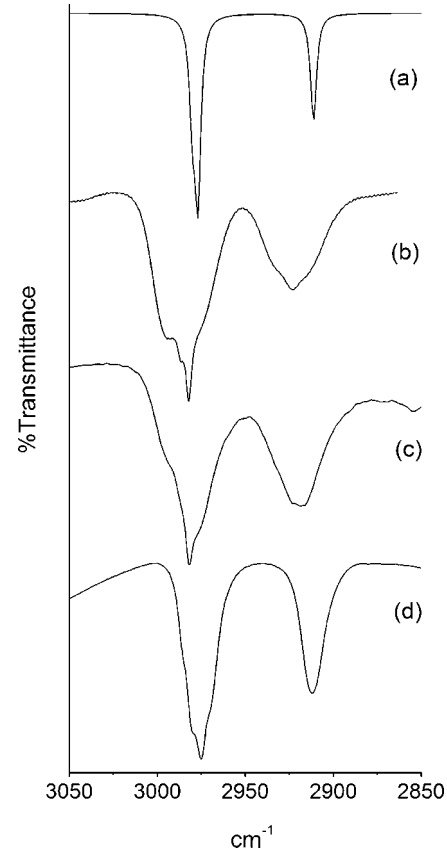

Figure 7. (a) WLS-scaled, (b) gas-phase room temperature, (c) liquid-phase room temperature, and (d) low-temperature FTIR spectra of TMG for the region between 3050 and 2850 cm^{-1}.

Methyl Group Modes. ***Stretching Modes.*** The vibrational spectra show the presence of C−H stretching vibrations in the region 3000−2900 cm^{-1}. Assignment of the observed bands was made mainly for comparison with the related iodotrimethylgermane compound.[31] The three C−H antisymmetric modes ν_{13}, ν_1, and ν_{14} were assigned to the three peaks located at 2994, 2986, and 2983 cm^{-1}, respectively, in the gas-phase infrared spectrum (Figure 7). The liquid and solid infrared spectra display bands centered at 2982 and 2975 cm^{-1} with several shoulders, which are listed in Table 1. The Raman spectrum in Figure 2 shows a depolarized band at 2980 cm^{-1}, which can be assigned to the ν_1 stretching mode. The C−H symmetric mode (ν_2) gives rise to a strongly polarized band at 2913 cm^{-1} in the Raman spectra, whereas in the low temperature infrared spectrum it was observed at 2911 cm^{-1}. The band at 2924 cm^{-1} and the shoulder at 2916 cm^{-1} observed for the gas phase, and at 2919 and at 2916 cm^{-1} for the liquid phase, were assigned to the ν_2 and ν_{15} vibrational modes, respectively.

Deformation Modes. Taking into account the previously reported spectra for iodotrimethylgermane[31] and the predictions made by calculation in Table 3, the two weak and broad features

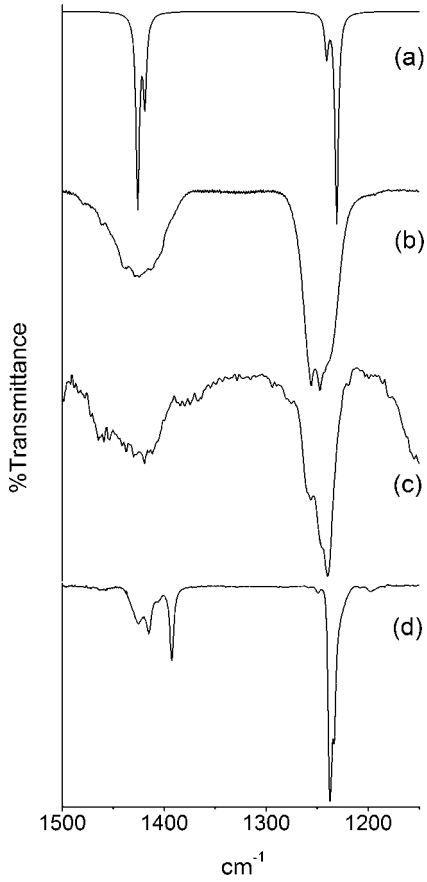

Figure 8. (a) WLS-scaled, (b) gas-phase room temperature, (c) liquid-phase room temperature, and (d) low-temperature FTIR spectra of TMG for the region between 1500 and 1150 cm^{-1}.

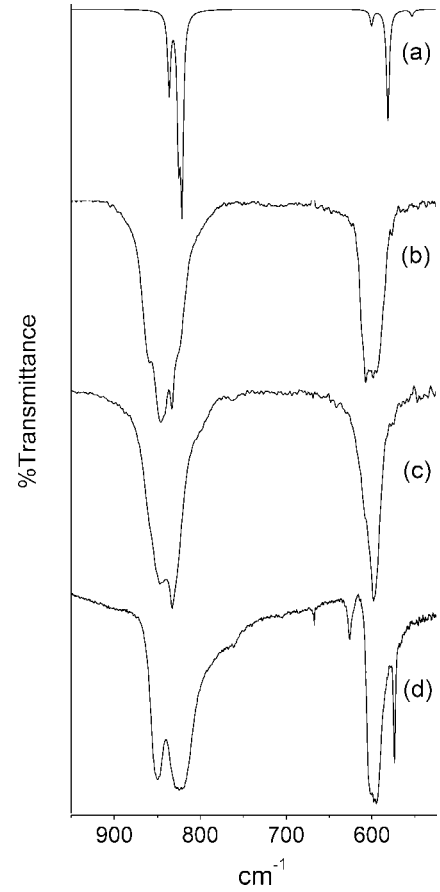

Figure 9. (a) WLS-scaled, (b) gas-phase room temperature, (c) liquid-phase room temperature, and (d) low-temperature FTIR spectra of TMG for the region between 960 and 500 cm^{-1}.

at 1425 and 1420 cm^{-1} accompanied by some shoulders for the gas and liquid infrared spectra can be assigned to the C−H antisymmetric deformation modes (ν_4, ν_{16}, and ν_{17}). These bands resolve clearly into individual components in the low-temperature spectrum (Figure 8), which shows bands at 1426 cm^{-1} attributed to the ν_4 mode, 1415 cm^{-1} attributed to the ν_{16} mode, and 1393 cm^{-1} assigned to the ν_{17} mode. The application of FSD to the Raman spectrum (Figure S2, Supporting Information) gives three bands at 1441, 1414, and 1384 cm^{-1}, in agreement with the bands observed for the solid phase. The C−H symmetric deformation modes appear as a medium band at 1256 cm^{-1} (ν_4) and a shoulder at 1227 cm^{-1} (ν_{17}) for the gas infrared spectrum. Likewise, in the liquid IR spectrum these modes were observed as a weak band at 1256 cm^{-1} and a shoulder at 1244 cm^{-1}. The IR spectrum for the solid phase shows more intense and closer peaks at 1238 cm^{-1} for the ν_4 mode and 1234 cm^{-1} for the ν_{17} mode, which also shows reverse relative intensity compared to that observed for both the gas and liquid spectra. The equivalent peaks in the Raman spectrum were observed at 1248 and 1235 cm^{-1}.

Rocking Modes. Three fundamental modes can be assigned as the CH_3 rocking modes. Two bands at 850 and 833 cm^{-1} were observed by previous authors[12] in this spectral region and they were assigned to a GeH deformation (ν_{21}) and to CH_3 rocking modes (ν_6 and ν_{20}), respectively. However, all the method and basis set combinations tested in this work (see Table S8, Supporting Information) are in agreement that the band at 850 cm^{-1} is due to a CH_3 rocking mode. Therefore, considering the WLS scaling predictions, the pair of bands observed in the gas-phase IR spectrum at 845 and 833 cm^{-1} can be attributed to the ν_{19} and ν_6 vibrational modes. These bands shift to 846 and 832 cm^{-1} for the liquid spectrum and to 850 and 831 cm^{-1} for the solid spectrum. On the other hand, no bands were observed in the earlier work[12] for the remaining ν_{20} rocking mode. Table 3 shows that the predicted splitting between the ν_6 and ν_{20} modes for the WLS scaling was 5 cm^{-1}. Consequently the shoulder observed in the gas-phase spectrum at 827 cm^{-1} with a splitting of 6 cm^{-1} generating the band at 833 cm^{-1} can be assigned to the ν_{20} mode. This assignment was confirmed by means of the low-temperature IR spectrum shown in Figure 9, where the band located at 825 cm^{-1} increases in intensity and separates from the others. The FSD of the Raman spectrum (Figure S2) in this region provides three bands located at 853, 840, and 828 cm^{-1}, belonging to the ν_{19}, ν_6, and ν_{20} vibrational modes.

Torsional Modes. The ν_{24} torsional mode of E symmetry is both infrared and Raman active and is predicted to be rather weak in both spectra. Therefore, a weak and broadband with a maximum at 132 cm^{-1} can be assigned to the ν_{24} torsional mode on the basis of the relative position and intensity predicted by the calculations in Table 3 for this vibration. This assignment is in accord with the previously reported torsional mode for $(CH_3)_3GeI$[31] observed at 112 cm^{-1}, which is expected to appear at a slightly lower frequency than for the hydrogen compound.

GeH Stretching Mode and GeC_3 Modes. The Ge−H stretching mode (ν_3) appears at almost the same frequency in all the infrared spectra. This mode displays a PQR band contour in the gas- and liquid-phase spectra as expected for a parallel vibration of a symmetric top molecule. These are shown in Figure 10. In the Raman spectrum this mode shifts to a lower frequency, appearing as a relatively strong polarized band at 2032 cm^{-1}.

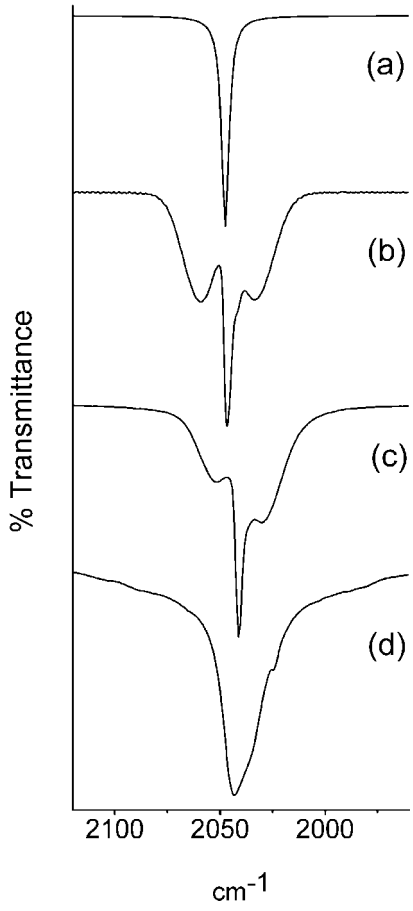

Figure 10. (a) WLS-scaled, (b) gas-phase room temperature, (c) liquid-phase room temperature, and (d) low-temperature FTIR spectra of TMG in the GeH stretching mode region.

The GeC_3 group vibrational modes are expected to appear below 700 cm^{-1}. The WLS scaling from Table 3 predicts the appearance of a band at 614 cm^{-1} corresponding to the ν_{21} mode. Imai et al.[12] observed a band at 624 cm^{-1}, which was assigned to the ν_{19} CH_3 rocking mode; however, as mentioned previously, the rocking modes were expected to appear at higher frequencies. In this study, there is a weak band at 626 cm^{-1} in the low-temperature infrared spectrum (Figure 9), but according to the calculations this band can be assigned to the GeC_3 antisymmetric deformation mode (ν_{21}), which gives a well-defined band at 629 cm^{-1} in the Raman spectrum. The GeC_3 antisymmetric (ν_{22}) and symmetric (ν_7) stretching modes give rise to two bands at 598 and 575 cm^{-1}, respectively, in the infrared spectra, which are in agreement with a depolarized band observed at 600 cm^{-1} and a polarized one at 575 cm^{-1} in the Raman spectrum. Although the GeC_3 antisymmetric stretching mode is mixed with the CH_3 rocking modes in the PED, a contribution of 72% confirms the assignment to this mode. The ν_8 and ν_{23} modes were earlier assigned to a band observed at 187 cm^{-1}.[12] In our Raman spectrum this band is located at 190 cm^{-1}, but taking into consideration the depolarization ratio (Table 1) and the relative intensities predicted for the WLS scaling, it can be assigned to the GeC_3 rocking mode (ν_{23}) of E symmetry. Because the band corresponding to the ν_8 mode is predicted to be weaker than that of the ν_{23} mode, it is probably overlapped and thus can not be observed. The combinations and overtone bands found in the vibrational spectra of TMG are reported in Table 4.

Calculation of Force Constants. The calculation of force constants was performed to obtain a detailed description of the vibrational modes that support the assignment of vibrational spectra. The scale factors proposed by Kalincsák and Pongor[19] were used as initial values and are shown in Table 5. As these factors have not been derived for compounds that contain germanium, they were refined using the SQM methodology.[16–19] For the refinement procedure the scale factors were grouped according to the nature and symmetry of the vibrational modes of the molecule and fitted by least-squares to the observed frequencies to reproduce the experimental vibrational data as well as possible. The B3LYP/6-31G* force field for TMG was scaled with 11 refined scale factors, decreasing the frequency deviations from an initial rmsd value of 36 cm^{-1} (with Kalincsák and Pongor[19] scale factors) to a final rmsd value of 4 cm^{-1}.

The resulting scaled frequencies are compared with the experimental data in Table 3. It is interesting to note that the differences between the theoretical and experimental frequencies are minimized when using different scaling methods. Application of the SQM method to the B3LYP/6-31G* force field decreases the rmsd values from 85 cm^{-1} to 36 cm^{-1} with use of the transferable Rauhut and Pulay[17] scale factors, to 36 cm^{-1} by using the Kalincsák and Pongor[19] scale factors, and to 4 cm^{-1} by using the refined scale factors obtained in this work. Also, application of the WLS method to the B3LYP/6-311+G** force

TABLE 4: Assignment of Combination Bands and Overtones Observed in the Vibrational Spectra of TMG

$IR_{(gas)}$	$IR_{(liq)}$	Raman	assignment
3826			$\nu_{13} + \nu_{20}$
3756			$\nu_2 + \nu_{20}$
3104		3106	$\nu_{15} + \nu_{23}$
3075			$\nu_{14} + \nu_{12}$
	2855		$\nu_{13} - \nu_{24}$
2825			$2\nu_{17}$
		2798	$\nu_{16} + \nu_{17}$
2478			$2\nu_{20} + \nu_{20}$
2236			$\nu_{17} + \nu_{20}$
1848			$\nu_3 - \nu_{23}$
1694			$2\nu_{19}$
	1656		$\nu_{15} - \nu_5$
1548	1542	1545	$\nu_1 - \nu_4$
		1087	$2\nu_{18} - \nu_{17}$
	1069		$\nu_5 - \nu_{23}$
	418		$\nu_5 - \nu_6$
398	397		$\nu_{18} - \nu_{19}$
389	384	385	$\nu_7 - \nu_{23}$

TABLE 5: Refined Scale Factors for TMG from the B3LYP/6-31G* Force Field

	scale factor	
vibrational mode[a]	initial[b]	final[c]
ν_a CH_3,	0.920	0.910
ν_s CH_3	0.920	0.910
ν GeH	0.920	1.060
δ_a CH_3	0.915	0.885
δ_s CH_3	0.915	0.895
ρ CH_3	0.915	0.882
$\delta_a GeC_3$	1.218	1.020
$\nu_a GeC_3$	1.042	0.990
$\nu_s GeC_3$	1.042	0.990
ρ GeC_3	1.218	1.090
$\delta_s GeC_3$	1.218	1.200
τ CH_3	0.831	0.800

[a] Key: ν, stretching; δ, angular deformation; ρ, rocking; τ, torsion; s, symmetric; a, antisymmetric. [b] Kalincsák and Pongor's scale factors, from ref 19. [c] Obtained after the refinement in this work.

TABLE 6: Internal Force Constants for TMG Calculated with B3LYP/6-31G*

coordinate	force constant[a]	
	initial[b]	final[c]
f(CH)	4.90	4.85
f(GeH)	2.16	2.44
f(GeC)	3.20	2.79
f(CGeC)	0.59	0.54
f(CGeH)	0.47	0.45
f(HCH)	0.44	0.42
f(HCGe)	0.36	0.35
f(HCGeH)	0.03	0.03
f(CGeC/CGeC)	−0.12	−0.11
f(CGeH/CGeH)	−0.06	−0.06
f(HCH/HCH)	−0.10	−0.10
f(HCGe/HCGe)	−0.06	−0.06

[a] Units are mdyn $Å^{-1}$ for stretchings and stretching/stretching interactions and mdyn Å rad $^{-2}$ for deformations and deformation/deformation interactions. [b] Calculated using Kalincsák and Pongor's scale factors included in Table 5. [c] Calculated using the scale factors obtained after the refinement procedure in this work.

field predicts frequencies with a deviation of just 15 cm^{-1}, whereas the unscaled predicted frequencies deviate ∼66 cm^{-1} from the experimental ones. The refined scale factors for the different types of motions and internal force constants obtained before and after the refinement procedure are shown in Tables 5 and 6. The detailed normal mode description in the potential-energy distribution (PED) obtained from the scaled B3LYP/6-31G* force field is presented in Table 3. The scaled force constant matrix is included in the Supporting Information (Table S9). In addition, the force constants, scale factors used to scale the theoretical force field, and the PED obtained for the B3LYP/6-311+G** level of theory and basis set are given in Tables S10−S12 (Supporting Information).

From the PED in Table 3 it can be seen that the C−H vibrational modes are strongly mixed, so it is common to find some discrepancies between theoretical methods (B3LYP/6-31G* and 6-311+G**) in relation to the relative positions of modes of similar frequency involving hydrogen atoms. The reverse order predicted for the ν_8 and ν_{23} GeC_3 vibrational modes would be more significant. However, the prediction obtained with the larger basis set was preferred for the assignment because the ν_8 mode cannot be observed in the experimental spectra.

Conclusions

The molecular structure for TMG was determined experimentally using gas electron diffraction studies combined with quantum mechanical calculations. New spectroscopic data were collected for the TMG by the measurement of its gas, liquid, and solid infrared spectra and its liquid Raman spectra. The depolarization ratios were used to identify some observed modes. The prediction of vibrational frequencies with the B3LYP hybrid method was sensitive to increasing basis set size and particularly to the inclusion of polarization functions. The 6-311+G** basis set also performed well in the calculation of infrared and Raman intensities when compared with the experimental spectra. Empirical corrections to the harmonic force field, such as the SQM and WLS scaling methodologies, have improved the calculated frequency quality and proved important in the assignment of the vibrational spectra. Overlapping frequency modes were resolved using low-temperature techniques and numerical spectral analysis, resulting in a complete assignment of the fundamental modes to the bands observed in the vibrational spectra of TMG.

Acknowledgment. A.B.A. thanks CIUNT (Consejo de Investigaciones, Universidad Nacional de Tucumán) and CONICET (Consejo Nacional de Investigaciones Científicas y Técnicas, R. Argentina) for financial support. M.L.R. thanks CONICET for the Ph.D. Fellowship. S.L.M. is grateful to the Royal Society of Edinburgh for a BP/RSE Personal Research Fellowship and to the EPSRC (grant number EP/D057167) for funding of the electron diffraction facilities. D.W.H.R., D.A.W., and H.E.R. also thank the EPSRC (grant number EP/C533649) for support.

Supporting Information Available: Correlation parameters, weighting points for off-diagonal weight matrices, scale factors for both camera distances for GED; HF, B3LYP, and MP2 geometric calculations; definition of symmetry coordinates; SQM matrix of symmetry force constants; amplitudes of vibration; correlation matrix and coordinates from the GED experiment; comparison of TMG with related halogenated germanes; experimental and calculated (B3LYP) vibrational frequencies with different basis sets. This material is available free of charge via the Internet at http://pubs.acs.org.

References and Notes

(1) Fish, R. H.; Kuivila, H. G. *J. Org. Chem.* **1966**, *31*, 2445.
(2) Piers, E.; Lemieux, R. *J. Chem. Soc., Perkin Trans. 1* **1995**, 3.
(3) Piers, E.; Lemieux, R. *Organomet.* **1995**, *14*, 5011.
(4) Spivey, A. C.; Gripton, C. J. G.; Noban, C.; Parr, N. J. *Synlett* **2005**, *14*, 2167.
(5) Coates, D.; Tedder, J. M. *J. Am. Soc., Perkin Trans.* **1978**, *11*, 725.
(6) Reichl, J.; Reichl, J. A.; Popoff, C. M.; Gallagher, L. A.; Remsen, E. E.; Berry, D. H. *J. Am. Chem. Soc.* **1996**, *118*, 9430.
(7) Patent application S.N 60/742,691.
(8) Zhang, Q.; Zhang, D.; Wang, S.; Gu, Y. *J. Phys. Chem. A* **2002**, *106*, 122.
(9) Arthur, N. L.; Miles, L. A. *Chem. Phys. Lett.* **1998**, *295*, 531.
(10) Durig, J. R.; Cheng, M. M.; Li, Y. S.; Turner, J. B. *J. Phys. Chem.* **1973**, *77* (2), 227.
(11) Van de Vondel, D. F.; Van der Kelen, G. P. *Bull. Soc. Chim. Belg.* **1965**, *74*, 467.
(12) Imai, Y.; Aida, K. *Bull. Chem. Soc. Jpn.* **1981**, *54*, 3323.
(13) Egorochkin, A. N.; Khorshev, S. Ya.; Ostasheva, N. S.; Sevastyanova, E. I. *J. Organomet. Chem.* **1976**, *105*, 311.
(14) McKean, D. C.; Torto, I.; Morrison, A. R. *J. Phys. Chem.* **1982**, *86* (3), 307.
(15) McKean, D. C.; MacKenzie, M. W.; Morrison, A. R. *J. Mol. Struct.* **1984**, *116*, 331.
(16) Pulay, P.; Fogarasi, G.; Pongor, G.; Boggs, J. E.; Vargha, A. *J. Am. Chem. Soc.* **1983**, *105*, 7037.
(17) Rauhut, G.; Pulay, P. *J. Phys. Chem.* **1995**, *99*, 3093.
(18) Rauhut, G.; Pulay, P. *J. Phys. Chem.* **1995**, *99*, 14572.
(19) Kalincsák, F.; Pongor, G. *Spectrochim. Acta A* **2002**, *58*, 999.
(20) Yoshida, H.; Takeda, K.; Okamura, J.; Ehara, A.; Matsuura, H. *J. Phys. Chem.* **2002**, *106*, 3580.
(21) Huntley, C. M.; Laurenson, G. S.; Rankin, D. W. H. *J. Chem. Soc., Dalton Trans.* **1980**, 954.
(22) Fleischer, H.; Wann, D. A.; Hinchley, S. L.; Borisenko, K. B.; Lewis, J. R.; Mawhorter, R. J.; Robertson, H. E.; Rankin, D. W. H. *Dalton Trans.* **2005**, 3221.
(23) Hinchley, S. L.; Robertson, H. E.; Borisenko, K. B.; Turner, A. R.; Johnston, B. F.; Rankin, D. W. H.; Ahmadian, M.; Jones, J. N.; Cowley, A. H. *Dalton Trans.* **2004**, 2469.
(24) Ross, A. W.; Fink, M.; Hilderbrandt, R. In *International Tables for Crystallography*; Wilson, A. J. C., Ed.; Kluwer Academic Publishers: Dordrecht, Boston, and London, 1992; Vol. C, p 245.
(25) (a) Kauppinen, J. K.; Moffatt, D. J.; Mantsh, H. H.; Cameron, D. G. *Appl Sepctrosc.* **1981**, *35*, 271. (b) Kauppinen, J. K.; Moffatt, D. J.; Cameron, D. G.; Mantsh, H. H. *Appl. Opt.* **1981**, *20*, 1866. (c) Kauppinen, J. K.; Moffatt, D. J.; Holberg, M. R.; Mantsh, H. H. *Appl. Spectrosc.* **1991**, *45*, 411.
(26) Griffiths, P. R.; Pierce, J. A.; Hongjin, G. In *Computer-Enhanced Analytical Spectroscopy*; Meuzelaar, H. L. C., Isenhour, T. L., Ed.; Plenum Press: New York, 1989; Chapter 2.
(27) Friesen, W. I.; Michaelian, K. H. *Appl. Spectrosc.* **1991**, *45*, 50.

(28) Michaelian, K. H.; Friesen, W. I.; Yariv, S.; Nasser, A. *Can. J. Chem.* **1991**, *69*, 1786.
(29) Spectrum Version 5.3, Elmer, Inc., 2005.
(30) Montejo, M.; Hinchley, S. L.; Ben Altabef, A.; Robertson, H. E.; Ureña, F. P.; Rankin, D. W. H.; López-Gónzalez, J. J. *Phys. Chem. Chem. Phys.* **2006**, *8*, 1.
(31) Roldán, M. L.; Brandán, S. A.; Masters (née Hinchley), S. L.; Wann, D. A.; Robertson, H. E.; Rankin, D. W. H.; Ben Altabef, A. *J. Phys. Chem. A* **2007**, *111*, 7200.
(32) Frisch, M. J.; Trucks, G. W.; Schlegel, H. B.; Scuseria, G. E.; Robb, M. A.; Cheeseman, J. R.; Montgomery, Jr., J. A.; Vreven, T.; Kudin, K. N.; Burant, J. C.; Millam, J. M.; Iyengar, S. S.; Tomasi, J.; Barone, V.; Mennucci, B.; Cossi, M.; Scalmani, G.; Rega, N.; Petersson, G. A.; Nakatsuji, H.; Hada, M.; Ehara, M.; Toyota, K.; Fukuda, R.; Hasegawa, J.; Ishida, M.; Nakajima, T.; Honda, Y.; Kitao, O.; Nakai, H.; Klene, M.; Li, X.; Knox, J. E.; Hratchian, H. P.; Cross, J. B.; Adamo, C.; Jaramillo, J.; Gomperts, R.; Stratmann, R. E.; Yazyev, O.; Austin, A. J.; Cammi, R.; Pomelli, C.; Ochterski, J. W.; Ayala, P. Y.; Morokuma, K.; Voth, G. A.; Salvador, P.; Dannenberg, J. J.; Zakrzewski, V. G.; Dapprich, S.; Daniels, A. D.; Strain, M. C.; Farkas, O.; Malick, D. K.; Rabuck, A. D.; Raghavachari, K.; Foresman, J. B.; Ortiz, J. V.; Cui, Q.; Baboul, A. G.; Clifford, S.; Cioslowski, J.; Stefanov, B. B.; Liu, G.; Liashenko, A.; Piskorz, P.; Komaromi, I.; Martin, R. L.; Fox, D. J.; Keith, T.; Al-Laham, M. A.; Peng, C. Y.; Nanayakkara, A.; Challacombe, M.; Gill, P. M. W.; Johnson, B.; Chen, W.; Wong, M. W.; Gonzalez, C.; Pople, J. A. *Gaussian03*, revision B.01, Gaussian, Inc.: Pittsburgh PA, 2003.
(33) Sipachev, V. A. *J. Mol. Struct. (THEOCHEM)* **1985**, *121*, 143.
(34) Fogarasi, G.; Zhou, X.; Taylor, P. W.; Pulay, P. *J. Am. Chem. Soc.* **1992**, *114*, 8191.
(35) Collier, W. B. *Program FCARTP (QCPE #631)*; Department of Chemistry, Oral Roberts University, Tulsa, OK, 1992.
(36) Keresztury, G.; Holly, S.; Varga, J.; Besenyei, G.; Wang, A. Y.; Durig, J. R. *Spectrochim. Acta A* **1993**, *49*, 2007.
(37) Navarro, A.; Lopez Gonzalez, J. J.; Garcia Fernandez, A.; Laczick, I.; Pongor, G. *Chem. Phys.* **2005**, *313*, 279.
(38) McLellan, A. L. *Tables of Experimental Dipole Moments*; W. H. Freeman: London, 1963.
(39) (a) Brain, P. T.; Morrison, C. A.; Parsons, S.; Rankin, D. W. H. *J. Chem. Soc., Dalton Trans.* **1996**, 4589. (b) Blake, A. J.; Brain, P. T.; McNab, H.; Miller, J.; Morrison, C. A.; Parsons, S.; Rankin, D. W. H.; Robertson, H. E.; Smart, B. A. *J. Phys. Chem.* **1996**, *100*, 12280. (c) Mitzel, N. W.; Rankin, D. W. H. *Dalton Trans.* **2003**, 3650.
(40) Aarset, K.; Page, E. M. *J. Phys. Chem. A* **2004**, *108*, 5474.
(41) Thomas, E. C.; Laurie, V. W. *J. Chem. Phys.* **1969**, *50*, 3512.
(42) Beagley, B.; Monaghan, J. J. *Trans. Faraday Soc.* **1970**, *66*, 2745.
(43) Hölbling, M.; Masters (née Hinchley), S. L.; Flock, M.; Baumgartner, J.; Hassler, K.; Robertson, H. E.; Wann, D. A. *Inorg. Chem.* **2008**, *47* (8), 3023.
(44) Koch, W.; Holthausen, M. C. *A Chemist's Guide to Density Functional Theory* , 2nd ed.; Wiley-VCH: Germany, 2002.

JP810988S